

Article

Synthesis, Spectroscopic Characterization, Molecular Docking and Biological Activity of Novel Secnidazole Metal Complexes

Wesam Abd El-Fattah ^{1,2,*} and Nuha Y. Elamin ^{1,3} 

¹ Department of Chemistry, College of Science, IMSIU—Imam Mohammad Ibn Saud Islamic University, P.O. Box 5701, Riyadh 11432, Saudi Arabia

² Department of Chemistry, Faculty of Science, Port-Said University, Port-Said 42521, Egypt

³ Department of Chemistry, Sudan University of Science and Technology, Khartoum P.O. Box 407, Sudan

* Correspondence: wabdufatah@imamu.edu.sa

Abstract: In this study, four new Secnidazole metal complexes have been synthesized through the reaction of Secnidazole drug with AuCl₃, PtCl₂, PdCl₂, AgNO₃ salts. The structures of the synthesized complexes were elucidated using elemental analysis, molar conductivity, thermal analysis, IR, ¹H-NMR and UV-Vis spectroscopy. The spectroscopic results confirm that Secnidazole drug act as a bidentate ligand, coordinated to the metal ion with N₃ of the imidazole ring and oxygen atom of OH group. The antimicrobial data revealed that the complexes possess a better antibacterial activity against most of the selected bacteria species than the free drug. In addition, the cytotoxic data showed that Ag-complex possesses a potent anticancer activity against MCF-7 cell line. The docking data showed that the synthesized complexes displayed a good and effective binding model against breast cancer protein (3hb5) which was confirmed by the low values of binding energy and multiple H-bonds.

Keywords: secnidazole; complexes; antibacterial activity; anticancer activity; molecular docking; MCF-7; HepG-2



Citation: Abd El-Fattah, W.; Elamin, N.Y. Synthesis, Spectroscopic Characterization, Molecular Docking and Biological Activity of Novel Secnidazole Metal Complexes. *Inorganics* **2022**, *10*, 156. <https://doi.org/10.3390/inorganics10100156>

Academic Editor: Marius Andruh

Received: 5 August 2022

Accepted: 19 September 2022

Published: 27 September 2022

Publisher's Note: MDPI stays neutral with regard to jurisdictional claims in published maps and institutional affiliations.



Copyright: © 2022 by the authors. Licensee MDPI, Basel, Switzerland. This article is an open access article distributed under the terms and conditions of the Creative Commons Attribution (CC BY) license (<https://creativecommons.org/licenses/by/4.0/>).

1. Introduction

Nitroimidazoles are considered one of the most important group of molecules that show diverse activity and are used for medical treatments. Many drugs that depend on the nitroimidazole ring are used in therapy for various bacterial infections [1]. Nitroimidazole-based drugs have also been used as anti-infective agents against a variety of diseases, including trichomonas, vaginitis, amebiasis, anaerobic bacteria, and treponemal bacteria [2].

Nitroimidazole is a considerable group of nitrogen heterocycles that are able to make several non-covalent bonds with biomolecules similar to DNA [3,4]. Owing to these characteristics, compounds containing nitroimidazole display a diversity of biological activities, such as antimicrobial, antiparasitic, and antitumor activities [1]. In addition, many nitroimidazole derivatives have been proven useful in the treatment of various diseases [5]. Secnidazole is a 5-nitroimidazoles derivative whose structure is similar to metronidazole [6]. It is used as an antimicrobial agent against some kinds of bacteria and parasites. Compared with other imidazole drugs, secnidazole is the most effective one, with few side effects [2].

In the area of coordination chemistry, nitroimidazole derivatives have usually been utilized as ligands chelating to various metal ions. They have received particular attention for numerous years due to the several ways that they can bonded to the metal in addition to their therapeutic properties [2]. It was previously reported [7] that synthesized imidazole complexes have important biological qualities, such as anticancer, anti-amoebic, antimicrobial, and also antiviral. Thus, metal complexes are considered the most widely utilized chemotherapeutic agents [8]. Furthermore, it was reported that the complexes of

transition metal salts with imidazole derivatives exhibited more antimicrobial activity than the ligands alone [9].

This prompted us to synthesize a series of novel Secnidazole complexes with Au(III), Pt(II), Pd(II), and Ag(I). The synthesized complexes were fully characterized by means of elemental analysis, molar conductivity, SEM, thermogravimetric analysis, UV, IR, and $^1\text{H-NMR}$ spectroscopy. The antimicrobial effects of the complexes were evaluated by a disk diffusion method. The cytotoxic activity of the new complexes toward HepG-2 and MCF-7 cell lines was assessed using the neutral red assay.

2. Results and Discussion

2.1. Synthesis of Secnidazole Complexes

Secnidazole complexes were synthesized by mixing Secnidazole solution with the corresponding metal salts solution in a 2:1 ligand-to-metal molar ratio. Then, drops of ammonium hydroxide solution were added, and the mixture was then refluxed. The proposed structures of the new synthesized complexes are shown in Figure 1.

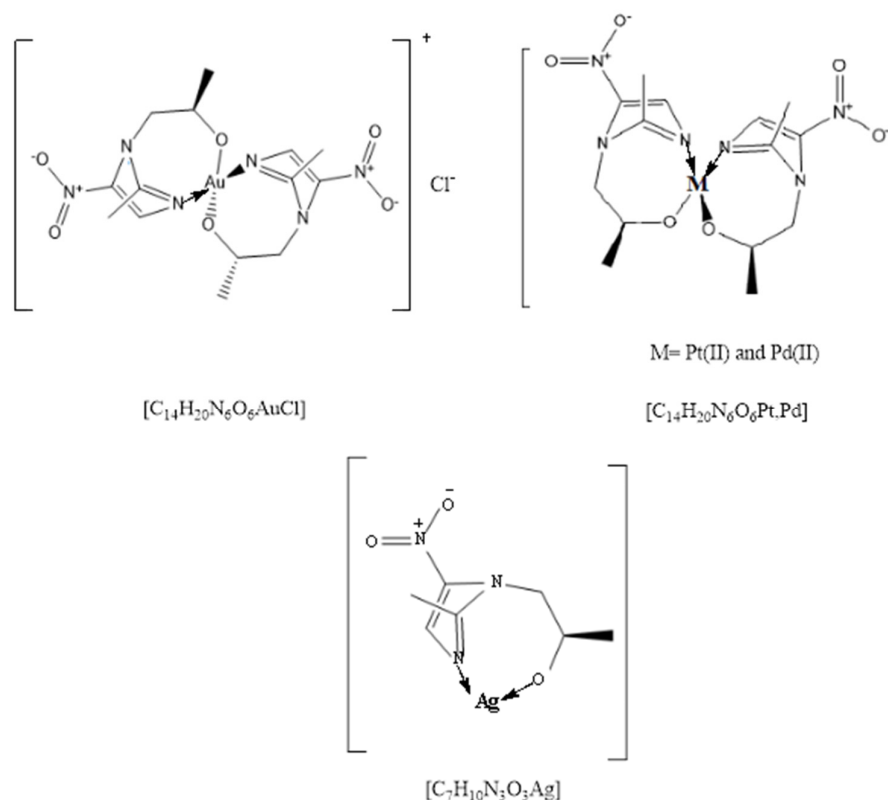


Figure 1. Proposed structure of the new synthesized complexes.

2.2. Elemental Analysis and Physical Properties

New metal complexes of Secnidazole were synthesized in good yields through the reaction of Secnidazole with AuCl_3 , PtCl_2 , PdCl_2 , and AgNO_3 . The colored, solid, isolated complexes are stable in air, having high melting points ranging from 200–350 °C and are insoluble in H_2O but soluble in organic solvents such as DMSO and DMF. The elemental analysis percent obtained for carbon, nitrogen, and hydrogen are matched with the proposed structures of the four new Secnidazole complexes, as shown in Table 1. Furthermore, the microanalytical data revealed that the stoichiometry between metal and ligand was found to be 1:2 in all complexes except Ag complex, which had a 1:1 stoichiometry.

Table 1. Physical properties of secnidazole complexes.

No.	Complexes Formula	Λ ($\text{Ohm}^{-1}\cdot\text{cm}^2\text{mol}^{-1}$)	Color	Yield%	m.p. °C	CHN (Found)		
						%C	%H	%N
1	$\text{C}_{14}\text{H}_{20}\text{N}_6\text{O}_6\text{AuCl}$	110.20	Light brown	91	350	27.96 (28.02)	3.32 (3.29)	13.98 (13.81)
2	$\text{C}_{14}\text{H}_{20}\text{N}_6\text{O}_6\text{Pt}$	13.10	black	74	260	29.81 (29.75)	3.54 (3.50)	14.90 (15.08)
3	$\text{C}_{14}\text{H}_{20}\text{N}_6\text{O}_6\text{Pd}$	11.60	Gray	80	300	35.38 (35.22)	4.21 (4.35)	17.69 (17.58)
4	$\text{C}_7\text{H}_{10}\text{N}_3\text{O}_3\text{Ag}$	16.80	Light gray	66	200	28.76 (28.85)	3.42 (3.38)	14.38 (14.26)

2.3. Conductance Measurements

The molar conductivities measurements of Secnidazole complexes were examined in DMSO solvent at 25 °C with a 1.0×10^{-3} M concentration. The molar conductivity values of the freshly prepared complexes recorded in Table 1 were found to be within the range of non-electrolytic values, except for the Au complex [10]. This result agreed with the analytical data assigned to the proposed structure for the synthesized complexes.

2.4. Infrared Spectra

The main IR bands of Secnidazole and its complexes are showed in Table 2. Secnidazole has many potential binding atoms that can chelate to metal ions at different sites. The assignments of the infrared bands were made by comparing the spectra of the complexes with the free drug. The IR spectral data of Secnidazole showed an intense absorption band at 3496 cm^{-1} , characteristic of the stretching vibration of the OH group. This band disappeared in the spectra of all synthesized complexes, revealing that the complex formation occurs through the deprotonation of the hydroxyl group. Furthermore, the bands observed at 1171 cm^{-1} corresponding to the $\nu(\text{CO})$ stretching modes in the free drug were shifted to lower frequencies in the complexes' spectra, which confirms its participation in the complexation with the metal ion. The synthesized complexes also displayed lower frequency shifts and intensity changes of the C=N group that appeared as a strong band at 1658 cm^{-1} in the ligand spectrum. This indicates the involvement of the N3 atom of the imidazole ring in the coordination with metal ions. Furthermore, new bands were observed at (521–562) and at (423–485) in the spectra of the studied complexes, corresponding to the M-O and M-N bonds, respectively.

Table 2. Main IR absorption bands of secnidazole and its complexes.

Compound	OH	C-O	C=N	C-N	M-O	M-N
Secnidazole	3500	1171	1658	1278	-	-
Au Complex	-	1150	1580	1264	521	423
Pt Complex	-	1158	1578	1260	535	485
Pd Complex	-	1148	1585	1258	544	470
Ag Complex	-	1160	1583	1262	562	447

2.5. Electronic Absorption Spectra

Electronic spectral data of the ligand and metal complexes are listed in Table 3 and the spectra are shown in Figure 2, measured in DMSO 10^{-4} M, in the range of 200 to 700 nm at room temperature. As shown in Figure 2, the electronic spectra of the free Secnidazole shows two types of transitions. The first one, which can be attributed to the $\pi-\pi^*$ transition, initially occurred at max 295 nm. It could be the result of transitions involving the imidazole ring's molecular orbitals. The complexes' spectra show a shift in this peak, which may be the result of the central metal atom receiving a single pair of electrons from the nitrogen of

the C=N compound. The second type of transition was observed at λ_{\max} 324 nm, which can be attributed to the $n\rightarrow\pi^*$ transition. This peak may be due to transitions involving molecular orbitals of the O-H or C=N chromophore with the imidazole ring. This band also changed after complexation, suggesting that the nitrogen atom in the imine group is likely coordinated with the metal ion. Table 3 contains the spectrum information for the free ligand secnidazole and its complexes in DMSO.

Table 3. The electronic spectral data of the free secnidazole ligand and its complexes.

Compound	λ_{\max} (nm)	Assignment
Secnidazole	295	$\pi\rightarrow\pi^*$ transition
	324	$n\rightarrow\pi^*$ transition
Au Complex	319	$n\rightarrow\pi^*$ transition
Pt Complex	330	$\pi\rightarrow\pi^*$ transition
	377	$n\rightarrow\pi^*$ transition
Pd Complex	285	$\pi\rightarrow\pi^*$ transition
	322	$n\rightarrow\pi^*$ transition
Ag Complex	355	$\pi\rightarrow\pi^*$ transition
	385	$\pi\rightarrow\pi^*$ transition
	376	$n\rightarrow\pi^*$ transition

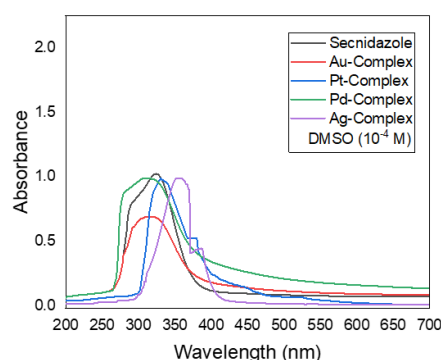


Figure 2. The UV spectra of the secnidazole ligand and its complexes.

2.6. $^1\text{H-NMR}$ Spectroscopy

The $^1\text{H-NMR}$ spectra of the Secnidazole ligand and its complexes were recorded in DMSO. The spectra show peaks at δ 8.00–8.19 ppm for Secnidazole and its complexes attributed to CH of the imidazole ring. The OH proton was observed at δ 5.05 ppm in the spectrum of Secnidazole and disappeared in the spectra of the synthesized complexes, which indicates the participation of the OH in the complexation with metal ions. The signal observed at δ 4.35–4.27 ppm in the spectra of Secnidazole, and its complexes was assigned to the (CH-OH) proton. Also, the peaks that appeared at δ 4.05–3.85 ppm in both spectra were characteristic of the protons of (CH₂-N). In addition, the two CH₃ groups give rise to two peaks at δ (2.45–2.58) and (1.17, 1.12) ppm in the spectra of Secnidazole and its complexes.

2.7. Scanning Electron Microscope (SEM)

The morphology of the obtained complexes was examined by SEM. It is possible to confirm that the complexes with the well-formed amorphous shape are the ones from the SEM images acquired, as shown in Figure 3. The complex monoliths' high particle sizes are also demonstrated. It is also crucial to remember that the monoliths are often made of micrometer-sized particles. There is no clear structure that can be defined because the complexes' single crystals could not be separated from any solutions.

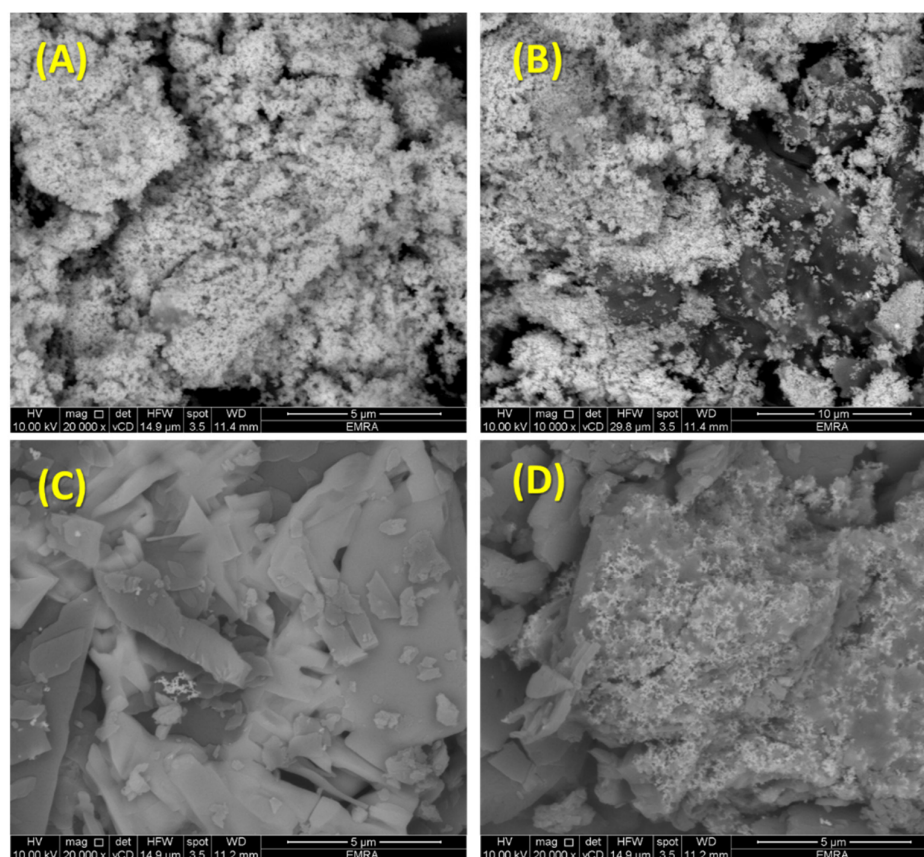


Figure 3. Representative SEM micrographs of the [Au(sec)₂Cl] (A) [Pt(sec)₂]; (B) [Pd(sec)₂]; (C) and [Ag(sec)]; (D) complexes.

2.8. Thermogravimetric Analysis

Thermal analysis curves of the free ligand Secnidazole and its [Au(sec)₂Cl], [Pt(sec)₂], [Pd(sec)₂], and [Ag(sec)] complexes are shown in Figure 4. The thermal decomposition of the free ligand secnidazole shows two steps. The first degradation step takes place between 151.28–191.98 °C and a weight loss of 11.46%. This loss can be attributed to the elimination of the OH group. The second step falls in the range of 247.03–267.02 °C, which can be assigned to loss of all organic molecules, with a weight loss of 88.27%. The thermal decomposition of [Au(sec)₂Cl] complex shows four degradation steps. The first step was located at 48.26–66.14 °C, with a weight loss of 2.38%. The loss in weight can be due to the adsorption of one water molecule. The second step falls in the range of 184.17–265.77 °C, with a weight loss of 40.06%. This step can be represented by the loss of two 1,2-dimethyl-5-nitro-1H-imidazole groups. The third step falls in the range of 315.47–352.44 °C, with a weight loss of 6.520%, which is assigned to the loss of the CH₃-CO group. The last step was located at 469.79–542.70 °C, with a weight loss of 4.644%. This step may be due to the loss of CH₃-C. The AuOCl is the final product, which remains stable up to 800 °C. The thermal decomposition of the [Pt(sec)₂] complex shows three degradation steps. The first step was located at 47.44–47.75 °C, with a weight loss of 1.717%. The loss in weight can be attributed to the adsorption of half of the water molecules. The second step falls in the range of 263.51–320.98 °C, with a weight loss of 29.945%. This step can be represented by the loss of one 2-methyl-5-nitro-1H-imidazole group. The third and the last step falls in the range of 445.84–477.83 °C, with a weight loss of 22.268%, which is attributable to the loss of the other 2-methyl-5-nitro-1H-imidazole group. The PtO is the final product, which remains stable up to 800 °C. The thermal decomposition of [Pd(sec)₂] complex shows three degradation steps. The first step falls in the range of 145.70–151.31 °C, with a weight loss of 9.536%. This step can be defined by the loss of nitro groups. The second step falls in the range of 310.31–329.08 °C, with a weight loss of 49.157% which is attributable to the loss of

two molecules of the 2-methyl-5-nitro-1H-imidazole group and one CH₃-CO group. The third step was located at 367.37–427.33 °C, with a weight loss of 9.125%. This step may be due to the loss of CH₃-C. The PdO is the final product, which remains stable up to 800 °C. The thermal decomposition of the [Ag(sec)] complex shows two degradation steps. The first step falls in the range of 190.88–249.96 °C, with a weight loss of 57.416%, which is attributable to the loss of the 2-methyl-5-nitro-1H-imidazole group and one CH₃ group. The second and the last step was located at 600.03–628.66 °C, with a weight loss of 10.977%. This step may be due to the loss of C-CH. The Ag₂O is the final product, which remains stable up to 800 °C.

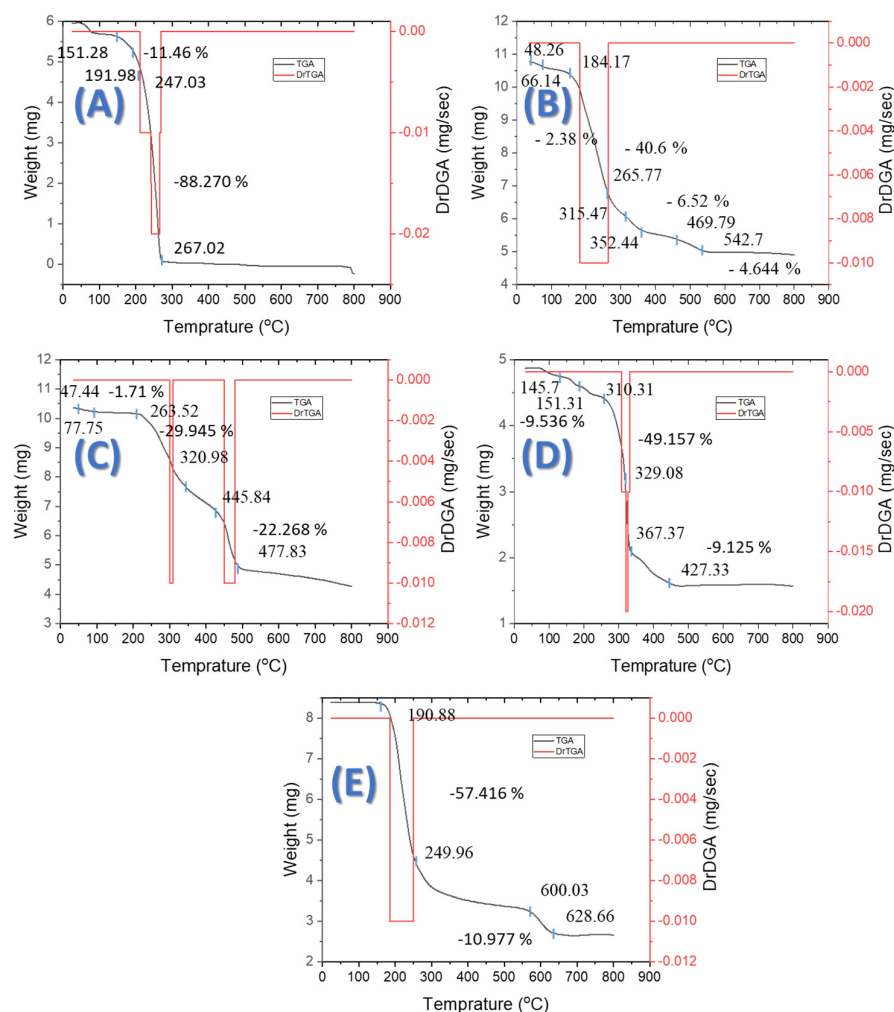


Figure 4. The TGA of the free ligand secnidazole (A) [Au(sec)₂Cl]; (B) [Pt(sec)₂]; (C) [Pd(sec)₂]; (D) and [Ag(sec)]; (E) complexes.

3. Biological Activity

3.1. Antimicrobial Activity

The antibacterial properties of Secnidazole and the four synthesized complexes were evaluated versus two species of gram-negative bacteria (*Klebsiella* and *E. coli*) and two species of gram-positive bacteria (*Staphylococcus epidermidis* and *Staphylococcus aureus*). The inhibition area was introduced in mm/mg and the antibacterial efficiency was compared with the standard drugs amoxicillin and ampicillin.

As shown in Table 4, the synthesized complexes possessed variable zones of inhibition against *Klebsiella*, *S. epidermidis*, and *S. aureus*, in which the highest inhibitory effect against *Klebsiella*, *S. epidermidis*, and *S. aureus* species was reported for the Pt complex, Ag complex, and Au and Pd complexes, respectively. On the other hand, all synthesized

complexes do not exhibit any activity against *E. coli* bacteria. The results also revealed that the synthesized complexes possess a better antibacterial activity against most of the selected bacteria species than the free drug. The highest activity of the complexes when compared with the standard drugs amoxicillin and ampicillin was found to be against the gram-negative bacteria *Klebsiella*, with a zone of inhibition ranging between 0.1 mm and 0.3 mm. On the basis of maximum inhibitory effect, the Pt complex exhibited the highest activity against *Klebsiella* species, as shown in Figure 5.

Table 4. Growth inhibition zone of the four synthesized complexes.

Sample	<i>Klebsiella</i>	<i>E. Coli</i>	<i>Staphylococcus Epidermidis</i>	<i>Staphylococcus aureus</i>
DMSO	0.0	0.0	0.0	0.0
Amoxicillin	0.4	0.3	0.9	0.4
Ampicillin	0.2	0.1	0.8	0.2
Secnidazole	0.0	0.0	0.0	0.0
Au Complex	0.2	0.0	0.1>	0.1
Pt Complex	0.3	0.0	0.1>	0.1>
Pd Complex	0.2	0.0	0.1>	0.1
Ag Complex	0.1	0.0	0.3	0.1>

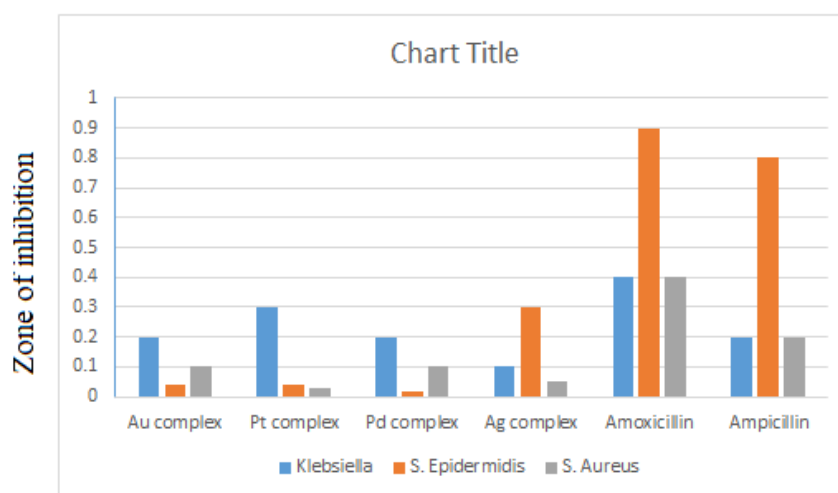


Figure 5. Antibacterial activities of the new synthesized complexes against *Klebsiella*, epidermidis, and *S. aureus*.

3.2. Anticancer Activities

The development of new selective anticancer drugs is receiving more attention in the field of therapeutics. In this study, all four synthesized complexes were screened for their cytotoxic effect against two types of human cancer cell lines: a hepatocellular carcinoma cell line (HepG-2) and a breast cancer cell line (MCF-7). The anticancer efficiency was estimated by IC₅₀ values using the neutral red assay. The untreated cells with media only were used as a negative control, whereas the positive standard control used was doxorubicin HCl with an IC₅₀ value (8 µg/mL). As shown in Table 5, the Au, Pt, and Pd complexes induce moderate cytotoxic activity against the breast cancer cell line only with IC₅₀ values of 21.6, 11.3, and 13.5 µg/mL, respectively. The Ag complex showed a potent anticancer activity against the breast cancer cell line (MCF-7), with IC₅₀ values of 7.4 µg/mL. At higher concentrations (50, 100 µg/mL) of the Ag complex, the cell viability percentage was very low. The results revealed that the Ag complex could be a promising potent anticancer agent against breast cancer. On the other hand, Au and Pd complexes showed low cytotoxic activity against the hepatocellular carcinoma cell line (HepG-2),

with IC₅₀ values > 100 µg/mL, whereas no cytotoxicity was reported for the Pt and Ag complexes, as shown in Table 5.

Table 5. IC₅₀ (µg/mL) values of the four complexes against MCF-7 and HepG-2 cell lines.

Complexes	MCF-7	HepG-2
Doxorubicin HCl	8.50	4.7
Secnidazole	-	-
Au Complex	21.6	>100
Pt Complex	11.3	-
Pd Complex	13.5	>100
Ag Complex	7.4	-

4. Docking Studies

A subset of artificial intelligence called machine learning aids researchers in finding novel compounds and pharmaceuticals as well as developing techniques to hasten the creation of new products. By using this tool, one may highlight items more accurately and with less time spent on calculations. Instead of wasting costly and possibly toxic molecules whose characteristics and behavior are unclear, the cost of development can be lowered by choosing good candidates for drug trials before starting in the lab. Molecular modelling for drug discovery is one area where artificial intelligence is used. A critical stage in both the design and implementation of medications as well as in comprehending biological processes is molecular docking. An automated software programmer is used to carry out this study. Use of the molecular docking approach simulates the process of molecules. By reducing the system's energy, this simulation suggests how to position a medication in relation to a protein to create the most stable combination.

The sequences of the various cell lines under study are extracted from the protein database as the initial step in the docking procedure (<http://www.pdb.org/> accessed in 1 August 2022). The B-chain, water molecules, and heteroatoms were deleted from these proteins' files in Discovery Studio Visualizer before they were stored in pdb format. The docking of a receptor and ligand can be done using a variety of software programs. The grid box's size was determined such that it would completely enclose the protein molecules [11]. In this section of our research, the interactions of the ligand and its complexes with the cell line breast cancer 17beta-hydroxysteroid dehydrogenase type 1 (3hb5) was examined to identify the best binding locations.

As shown in Tables 6–10, all the energy of interaction has a negative charge, which indicates a good and effective binding model between the synthesized complexes with the protein. These interactions take place through several types of bonds, such as H-bonds, van der Waals, conventional hydrogen bonding, carbon–hydrogen, pi-donor hydrogen and pi-alkyl bonds. They form between the nitrogen atom of the azomethine group in addition to the oxygen atoms of the hydroxyl groups and nitro group of the complexes and the amino acid residues of the different receptors. Furthermore, some complexes bind with its metal with the amino acid of the protein.

Table 6. Binding energy of the interaction of secnidazole.

Protein	Receptor	Interaction	Distance	E (kcal/mol)
Breast cancer ID: 3hb5	VAL 188	H-acceptor	3	−2.6

Table 7. Binding energy of the interaction with Ag- Complex.

Protein	Receptor	Interaction	Distance	E (kcal/mol)
Breast cancer ID: 3hb5	SER 12	H-donor	3.41	−0.7
	THR 190	H-donor	3.21	−1
	SER 12	H-acceptor	3.41	−0.6
	GLY 15	H-acceptor	2.98	−3
	ASN 90	H-acceptor	2.91	−3.1

Table 8. Binding energy of the interaction with Au complex.

Protein	Receptor	Interaction	Distance	E (kcal/mol)
Breast cancer ID: 3hb5	GLY 92	H-acceptor	3.2	−1.3
	LYS 159	H-acceptor	3.15	−2
	GLY 92	H-acceptor	3.44	−1.2

Table 9. Binding energy of the interaction with Pd complex.

Protein	Receptor	Interaction	Distance	E (kcal/mol)
Breast cancer ID: 3hb5	SER 142	H-donor	2.91	−4.3
	SER 142	H-acceptor	3.23	−0.8
	THR 190	H-acceptor	3.05	−1.7

Table 10. Binding energy of the interaction with Pt complex.

Protein	Receptor	Interaction	Distance	E (kcal/mol)
Breast cancer ID: 3hb5	VAL 188	H-acceptor	3.3	−0.6
	SER 142	H-acceptor	2.7	−1.1
	MET 193	H-acceptor	3.7	−0.7

The binding free energy docking scores (S) and root-mean-square deviations (RMSD) of atomic positions for Secnidazole and the synthesized complexes with the 17 β -hydroxysteroid dehydrogenase type 1 (3hb5) protein are presented in Table 11. The estimated binding scores of the free ligand Secnidazole were calculated as −5.52 kcal/mol for the 3hb5 protein, whereas the binding score values of the synthesized Ag, Pt, Pd, and Au complexes were −8.36, −8.31, −7.92, and −5.88 kcal/mol, respectively. Notably, the results revealed high docking scores for the complexes compared to those for the free ligand, especially for the Ag complex. This indicates that the synthesized metal complexes enhance the binding affinity of the free ligand. All the 2D, 3D, and side interactions of the drug and its complexes with the target are illustrated in Tables 12–14.

Table 11. Docking score and energy of the compounds and 3hb5 breast cancer protein.

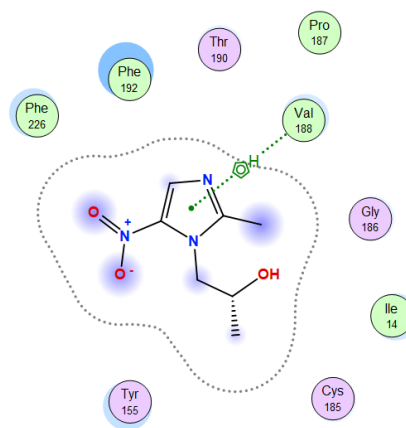
Compound	S	rmsd_Refine	E_Conf	E_Place	E_Score1	E-Refine	E_Score2
Secnidazole	−5.11	1.48	6.27	−55.58	−8.23	−17.35	−5.11
	−5.07	1.61	7.34	−57.05	−8.06	−26.67	−5.07
	−5.01	1.89	5.44	−51.78	−8.04	−23.10	−5.01
	−5.00	0.94	7.24	−49.75	−8.46	−17.36	−5.00
	−4.95	0.84	5.87	−51.82	−8.20	−20.08	−4.95

Table 11. Cont.

Compound	S	rmsd_Refine	E_Conf	E_Place	E_Score1	E-Refine	E_Score2
Au complex	−6.87	1.32	216.30	−52.50	−9.90	−25.52	−6.87
	−4.77	0.76	214.28	−76.74	−10.78	−26.23	−4.77
	−4.76	2.19	227.67	−47.30	−10.66	−33.73	−4.76
	−4.74	1.65	214.07	−53.80	−10.04	−21.61	−4.74
	−4.70	1.06	215.14	−61.43	−10.15	−18.83	−4.70
Pt complex	−7.48	2.49	149.63	−55.58	−10.83	−37.00	−7.48
	−7.03	1.94	147.23	−69.33	−9.63	−34.12	−7.03
	−6.91	0.99	147.06	−56.01	−9.56	−23.91	−6.91
	−6.79	1.39	157.33	−43.52	−10.23	−25.46	−6.79
	−6.78	2.19	158.43	−54.43	−10.47	−23.45	−6.78
Pd complex	−7.43	1.58	134.52	−60.31	−10.19	−35.53	−7.43
	−6.84	2.18	154.23	−47.58	−9.38	−22.29	−6.84
	−6.63	1.68	123.10	−54.16	−9.68	−31.50	−6.63
	−6.57	1.25	150.12	−47.46	−9.12	−22.53	−6.57
	−6.52	1.81	132.06	−65.60	−10.14	−33.36	−6.52
Ag complex	−7.87	0.97	232.12	−43.69	−7.10	−21.43	−7.87
	−7.30	2.48	232.46	−57.20	−8.46	−17.48	−7.30
	−7.06	1.17	233.05	−52.75	−6.99	−13.68	−7.06
	−7.05	1.59	234.16	−45.31	−7.01	−13.85	−7.05
	−7.02	0.67	232.78	−57.80	−7.61	−15.75	−7.02

Table 12. 2D and site interaction of the ligand and its metal complexes with 3hb5 protein.

Secnidazole



Au complex

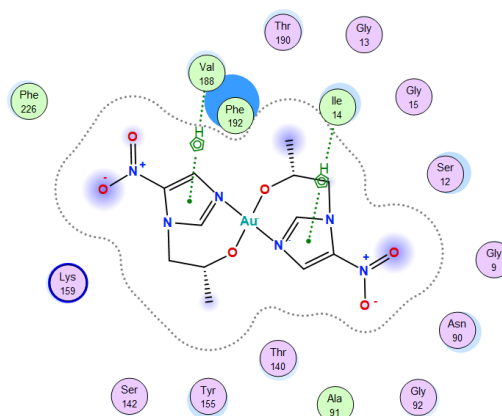
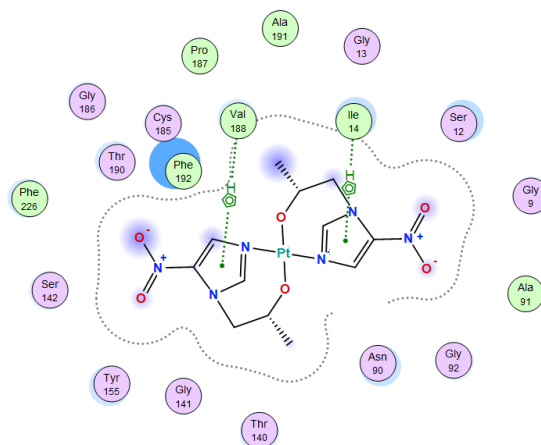
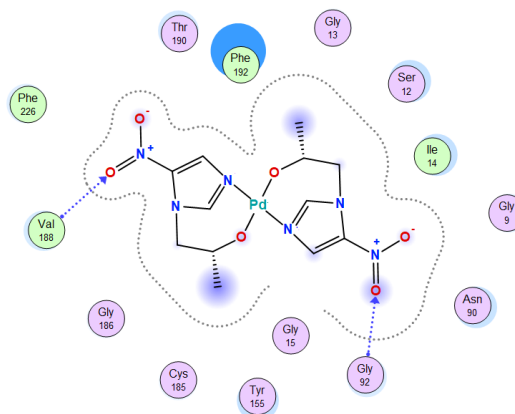


Table 12. Cont.

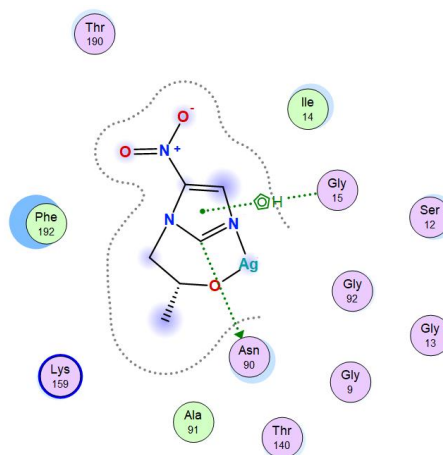
Pt complex



Pd complex



Ag complex



- | | | | |
|-------------------|--------------------|-------------------|--------------|
| polar | sidechain acceptor | solvent residue | arene-arene |
| acidic | sidechain donor | metal complex | arene-H |
| basic | backbone acceptor | solvent contact | arene-cation |
| greasy | backbone donor | metal/ion contact | |
| proximity contour | ligand exposure | receptor exposure | |

Table 13. 3D and site interaction of the ligand and its metal complexes with 3hb5 protein.

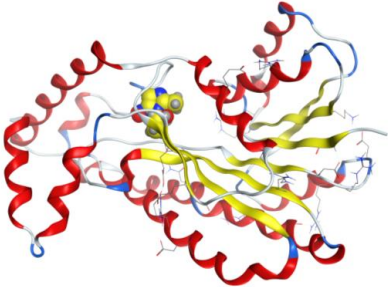
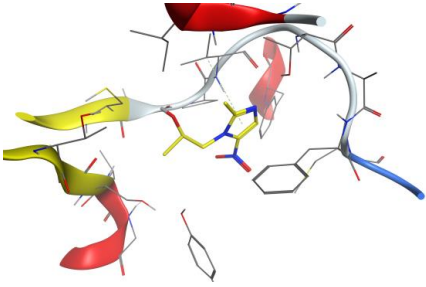
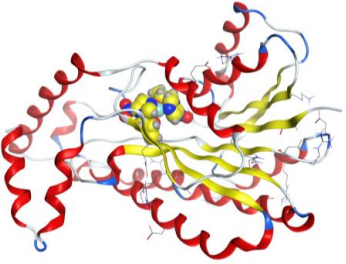
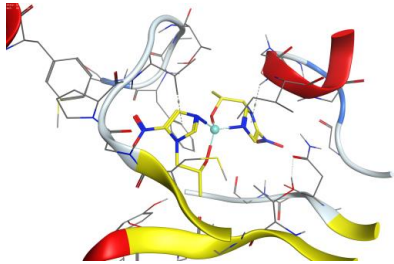
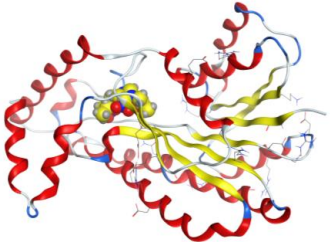
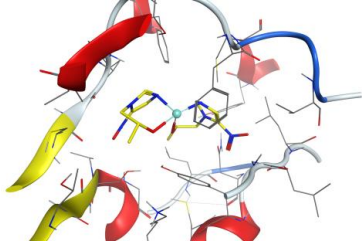
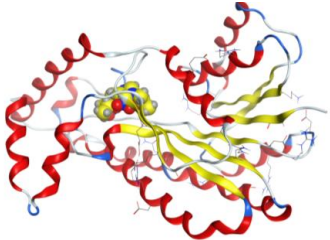
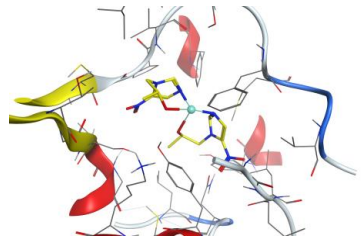
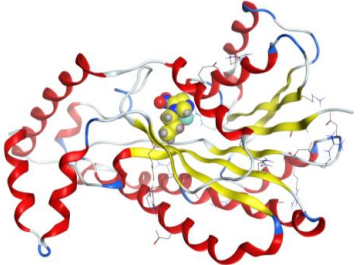
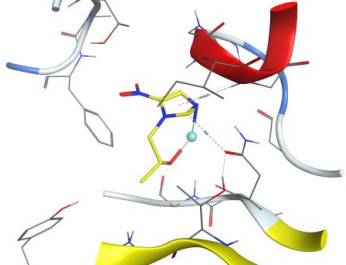
Secnidazole		
Au complex		
Pt complex		
Pd complex		
Ag complex		

Table 14. Docking interaction of the ligand and its metal complexes with 3hb5 protein.

Compound	Ligand	Receptor	Interaction	Distance	E (kcal/mol)
Secnidazole	5-ring	CB VAL 188 (X)	pi-H	4.30	−0.5
Au complex	5-ring	N ILE 14 (X)	pi-H	3.97	−1.1
	5-ring	CB VAL 188 (X)	pi-H	4.01	−0.6
Pt complex	5-ring	N ILE 14 (X)	pi-H	4.26	−1.0
	5-ring	CB VAL 188 (X)	pi-H	4.14	−0.8
Pd complex	O 37	N GLY 92 (X)	H-acceptor	2.87	−1.2
	O 40	N VAL 188 (X)	H-acceptor	2.98	−1.2
Ag complex	C 5	OD1 ASN 90 (X)	H-donor	3.40	−1.5
	5-ring	N GLY 15 (X)	pi-H	4.48	−4.1

5. Materials and Methods

5.1. Reagents

Secnidazole, the metal salts (AuCl₃, PtCl₂, PdCl₂, AgNO₃), and the solvents used in this work were obtained from Aldrich and were of analytical grade. All chemicals were used as obtained without further purification.

5.2. General Procedure for the Preparation of Secnidazole Complexes

Au(III), Pt(II), Pd(II), and Ag(I) complexes of Secnidazole were synthesized according to the following method. One mmol of the corresponding metal salts solution in methanol was added to a solution of two mmol of Secnidazole in 20 mL methanol; then, drops of ammonium hydroxide solution were added. The solution was then refluxed with stirring for 5 h. The solid complexes were formed at the bottom of the flask. The mixture was cooled and filtered; then, the precipitate was washed with methanol and then dried overnight to give four colored products.

5.2.1. [Au(sec)₂Cl] (1)

Solid gold (III)chloride (0.34 g, 1.12 mmol), Secnidazole (0.37 g, 2 mmol) in methanol. The solution changed from orange to brown; a yellow brown ppt was formed. Yield: 91%. Elemental Anal. Calc. for C₁₄H₂₀N₆O₆AuCl: C, 27.96; H, 3.32; N, 13.98. Found: C, 28.02; H, 3.29; N, 13.81%. Selected IR peaks (cm^{−1}): 2981, 2878 (w), 1580 (s), 1548 (m), 1264 (s), 1150 (s).

5.2.2. [Pt(sec)₂] (2)

Solid platinum (II) chloride (0.266 g, 1.00 mmol), Secnidazole (0.37 g, 2 mmol) in methanol. The solution changed from green to black; a black ppt was formed. Yield: 74%. Elemental Anal. Calc. for C₁₄H₂₀N₆O₆Pt: C, 29.81; H, 3.54; N, 14.90. Found: C, 29.75; H, 3.50; N, 15.08%. Selected IR peaks (cm^{−1}): 2968, 2850 (w), 1578 (s), 1542 (m), 1260 (s), 1158 (s).

5.2.3. [Pd(sec)₂] (3)

Solid palladium (II) chloride (0.22 g, 1.03 mmol), Secnidazole (0.37 g, 2 mmol) in methanol. The solution changed from green to black; a black solid was formed. Yield: 80%. Elemental Anal. Calc. for C₁₄H₂₀N₆O₆Pd: C, 35.38; H, 4.21; N, 17.69. Found: C, 35.22; H, 4.35; N, 17.58%. Selected IR peaks (cm^{−1}): 2975, 2871 (w), 1585 (s), 1538 (m), 1258 (s), 1148 (s).

5.2.4. [Ag(sec)] (4)

Solid silver (I) nitrate (0.17 g, 1.00 mmol), Secnidazole (0.37 g, 2 mmol) in methanol. The solution changed from colorless to light grey; a grey solid was obtained. Yield: 66%. Elemental Anal. Calc. for C₇H₁₀N₃O₃Ag: C, 28.76; H, 3.42; N, 14.38. Found: C, 28.85;

H, 3.38; N, 14.26%. Selected IR peaks (cm^{-1}): 2981, 2886 (w), 1583 (s), 1529 (m), 1262 (s), 1160 (s).

5.3. Spectroscopic Measurements

The melting points were measured on a MEL-TEMP II melting point apparatus. The conductivity measurement of the synthesized complexes solutions (10^{-3} M) in DMSO was measured using a Jenway 4010 conductivity meter. Elemental (CHN) analysis was determined by an elemental analyzer 1106 in the Micro-analytical Unit at the Faculty of Science, Ain Shams University, Egypt. Infrared spectra were recorded in the range $4000\text{--}400\text{ cm}^{-1}$ using a Perkin Elmer FT-IR Spectrum 400 spectrophotometer. $^1\text{H-NMR}$ spectra of the ligand and its complexes were carried out on a Bruker 600 MHz spectrometer using DMSO- d_6 . The UV-Vis spectra were evaluated in DMSO using a Jenway 6405 Spectrophotometer. The thermal studies TGA were carried out on a Shimadzu TGA-50H thermal analyzer. In addition, the morphology of the complexes was examined using scanning electron microscopy (JSM, 6510 LV, JEOL). Microbiological analysis was recorded using a disk diffusion method. Anticancer activity was determined at the Regional Center for Mycology and Biotechnology, Al-Azhar University, Cairo, Egypt. For molecular docking, affinity maps of protein were generated using the MOE.2015.10 software (Montreal, QC, Canada), which used a docking algorithm to find the correct location of the ligand with regards to its receptor.

5.4. Antimicrobial Activity

In this study, the antibacterial activity of the four synthesized complexes was investigated against *Escherichia coli*, *Klebsiella*, *Staphylococcus aureus*, and *Staphylococcus epidermidis* using a disk diffusion method [12]. The sterilized media was melted at 373 K, then poured onto the plates after cooling to 329 K and allowed to solidify. The bacterial cultures were preserved in the same media at $30 \pm 3\text{ }^\circ\text{C}$ for 18–24 h. A total of 0.1 mL of the cell suspension was impregnated into each plate and spread homogeneously; then, the medium surface was left to dry. A total of 5 mm Whatman filter paper discs were deposited on the top of the dry surface. Then, a 5 μL solution of the tested complexes in DMSO was added in different concentrations and incubated for 24–48 h. After inoculation, the zone of inhibition (mm) was measured for all complexes. DMSO solvent as a negative control showed no zone of inhibition against the tested bacteria.

5.5. Cytotoxicity Assay

In vitro, the cytotoxicity of the tested new Secnidazole complexes was evaluated towards two human cancer cell lines—a hepatocellular carcinoma cell line (HepG-2) and a breast cancer cell line (MCF-7)—using the standard neutral red uptake assay [13]. These cell lines were purchased from the Egyptian Holding Company for Biological Products & Vaccines (VACSERA), Giza, Egypt. Briefly, cells were tested using different concentrations of the synthesized complexes (25–200 $\mu\text{g}/\text{mL}$). The medium was aspirated, and cells were twice washed with phosphate-buffered saline, then incubated for 3 h after adding 50 $\mu\text{g}/\text{mL}$ of neutral red. Then, the medium was washed with a solution comprising 0.5% CH_2O and 1% CaCl_2 . Cells were then incubated for 20 min at $37\text{ }^\circ\text{C}$ in a mixture of acetic acid (1%) and ethanol (50%) to extract the dye. The absorbance of viable cells was measured at a wavelength of 550 nm. In addition, the effect of the drug concentration on the survival of the cells was plotted to obtain the survival curve of each tumor cell line after treatment with each complex. The 50% inhibitory concentration (IC₅₀) was estimated from the graphic plots of the dosage response curve for each concentration.

6. Conclusions

There is currently considerable interest in the development of metal-complex-based drugs with therapeutic properties in the medicinal chemistry area. The present work describes the synthesis and in vitro antimicrobial and anticancer activity of Secnidazole and its Au(III), Pt(II), Pd(II), and Ag(I) complexes. These coordinated complexes showed better

antibacterial activity than the free drug, especially towards the gram-negative bacteria *Klebsiella*. In addition, the synthesized complexes exhibit improved cytotoxic activity (IC₅₀ values) against a breast cancer cell line (MCF-7) when compared to the standard control, doxorubicin HCl. The molecular docking study of the interaction between the synthesized complexes and the selected cell line showed a good binding model with 3hb5 protein. Therefore, the synthesized complexes can be the starting point for a promising candidate against many diseases.

Author Contributions: Conceptualization, W.A.E.-F. and N.Y.E.; methodology, W.A.E.-F.; software, N.Y.E.; validation, W.A.E.-F. and N.Y.E.; formal analysis, N.Y.E.; investigation, W.A.E.-F.; resources, W.A.E.-F.; data curation, N.Y.E.; writing—original draft preparation, W.A.E.-F.; writing—review and editing, W.A.E.-F. and N.Y.E.; visualization, N.Y.E.; supervision, W.A.E.-F.; project administration, W.A.E.-F. and N.Y.E.; funding acquisition, W.A.E.-F. All authors have read and agreed to the published version of the manuscript.

Funding: This research was funded by the Deanship of Scientific Research, Imam Mohammad Ibn Saud Islamic University, Saudi Arabia, Grant No. (20-13-12-023).

Data Availability Statement: All relevant data are within the manuscript.

Acknowledgments: This research was supported by the Deanship of Scientific Research, Imam Mohammad Ibn Saud Islamic University, Saudi Arabia, Grant No. (20-13-12-023).

Conflicts of Interest: The authors declare no conflict of interest.

References

1. Ang, C.W.; Jarrad, A.M.; Cooper, M.A.; Blaskovich, M.A. Nitroimidazoles: Molecular fireworks that combat a broad spectrum of infectious diseases. *J. Med. Chem.* **2017**, *60*, 7636–7657. [[CrossRef](#)] [[PubMed](#)]
2. Soledad, B.L.; Isabel, G.M.; Pilar, G.M.; Marcos, F.; Marcos, F.A.; Noráh, B.B. Synthesis, characterization, and biological activity of cobalt(II), nickel(II), copper(II), and zinc(II) complexes of secnidazole. *Inorg. Chim. Acta* **2013**, *397*, 94–100.
3. Ling, Z.; Xin, M.P.; Guri, L.V.D.; Rong, X.G.; Cheng, H.Z. Comprehensive review in current developments of imidazole-based medicinal chemistry. *Med. Res. Rev.* **2014**, *34*, 340–437.
4. Zhang, H.Z.; Gan, L.L.; Wang, H.; Zhou, C.H. New Progress in Azole Compounds as Antimicrobial Agents. *Mini-Rev. Med. Chem.* **2017**, *17*, 122–166. [[CrossRef](#)] [[PubMed](#)]
5. Zhen, Z.L.; Lavanya, G.; Vijai, K.; Reddy, T.; Wei, W.G.; Cheng, H.Z. Discovery of novel nitroimidazole enols as *Pseudomonas aeruginosa* DNA cleavage agents. *Bioorg. Med. Chem.* **2017**, *25*, 6511–6522.
6. Huang, X.S.; Wang, L.S.; Yin, Y.; Li, W.M.; Duan, M.; Ran, W.; Zhu, H.L. Synthesis, characterization and bioactivity research of a derivative of secnidazole: 1-(2-chloropropyl)-2-methyl-5-nitro-1H-imidazole. *J. Chem. Crystallogr.* **2011**, *41*, 1360–1364. [[CrossRef](#)]
7. López, S.H.; Londoño, L.M.E.; Garza, V.R.; Poblano, M.I.I.; Granada, M.P.; Gracia, M.I.; Barba, B.N. Synthesis, structure and biological activities of cobalt(II) and zinc(II) coordination compounds with 2-benzimidazole derivatives. *J. Inorg. Biochem.* **2008**, *102*, 1267. [[CrossRef](#)] [[PubMed](#)]
8. Clarke, M.J.; Zhu, F.; Frasca, D.R. Non-platinum chemotherapeutic metallopharmaceuticals. *Chem. Rev.* **1999**, *99*, 2511. [[CrossRef](#)] [[PubMed](#)]
9. Selwin, J.R.; Sivasankaran, N.M. Synthesis, characterization and antimicrobial activity of transition metal complexes with the schiff base derived from imidazole-2-carboxaldehyde and glycylglycine. *J. Coord. Chem.* **2009**, *62*, 319–327. [[CrossRef](#)]
10. Geary, W.J. The use of conductivity measurements in organic solvents for the characterization of coordination compounds. *Coord. Chem. Rev.* **1971**, *7*, 81–122. [[CrossRef](#)]
11. El-Bindary, A.A.; El-Desouky, M.G.; El-Afify, M.A.M. Thermal and Spectroscopic Studies of Some Prepared Metal Complexes and Investigation of their Potential Anticancer and Antiviral Drug Activity against SARS-CoV-2 by Molecular Docking Simulation. *Biointerface Res. Appl. Chem.* **2021**, *12*, 1053–1075.
12. Bauer, A.W.; Kirby, W.A.; Sherris, C.; Turck, M. Antibiotic susceptibility testing by a standardized single disc method. *Am. J. Clin. Pathol.* **1996**, *45*, 493–496. [[CrossRef](#)]
13. Repetto, G.; del Peso, A.; Zurita, J.L. Neutral red uptake assay for the estimation of cell viability/cytotoxicity. *Nat. Protoc.* **2008**, *3*, 1125–1131. [[CrossRef](#)] [[PubMed](#)]